Available online at www.sciencedirect.com
ScienceDirect
Journal of Nuclear Materials 373 (2008) 1–8
journal of nuclear materials
www.elsevier.com/locate/jnucmat

Structural, thermal, electrical and magnetic properties of Eurofer 97 steel

K. Mergia [a,*], N. Boukos [b]

[a] Institute of Nuclear Technology and Radiation Protection, National Centre for Scientific Research 'Demokritos', 15310 Aghia Paraskevi Attikis, Greece
[b] Institute of Materials Science, National Centre for Scientific Research 'Demokritos', 15310 Aghia Paraskevi Attikis, Greece

Received 5 April 2006; accepted 30 March 2007

Abstract

The structure of Eurofer 97 has been determined by diffraction and electron microscopy techniques. The magnetic (coercive field, saturation and remanence magnetization and Curie temperature), electrical and thermal properties of Eurofer 97 steel are reported in the temperature range from room temperature up to 900 K. The experimental data are described by empirical equations and are compared with data from similar steel alloys.

PACS: 75.60.Ej; 67.80.Gb; 61.12.Ld; 28.52.−s

1. Introduction

Thermal, electrical and magnetic properties of materials are critical to the success of computational models that predict materials behaviour and processing at elevated temperatures. Reduced Activation Ferritic Martensitic (RAFM) steel is the primary choice material for first wall and breeding blanket structural application for ITER and in future fusion power plants. These steels have been developed in order to simplify special waste storage of highly radioactive structures of fusion reactor after service. With this objective some alloying elements such as Mo, Nb and Ni present in the commercial martensitic steels have been replaced by other elements which exhibit faster decay of induced radioactivity such as Ta, W and V [1]. Eurofer 97 is the reference RAFM steel developed for the requirements of the European fusion technology program [2–9]. Its chemical composition has been designed and optimized to obtain good metallurgical properties comparable to the conventional Cr–Mo steels and reduced long term radioactivity.

The main aim of this paper is to evaluate the thermal, electrical and magnetic properties of Eurofer 97 and to compare them with those of the reduced activation martensitic steel F82H, a material studied as a candidate structural material for fusion reactors [10].

2. Experimental procedure

The material used in this study is the low activation ferritic/martensitic steel Eurofer 97 with the following chemical composition in wt%: 0.11C, 8.9Cr, 0.42Mn, 0.19V, 1.10W, 0.14Ta, balance Fe. The samples were obtained from forged bar (Heat E83699) produced by BÖHLER EDELSTAHL GmbH in Austria. The forged bars (E83699) treatments are 979 °C/1 h 51 min/air cooled plus 739 °C/3 h 42 min/air cooled.

The structure of the Eurofer was determined by neutron and X-ray diffraction and TEM observations. The neutron diffraction measurements were carried out at the neutron diffractometer at the Greek Research Reactor at N.C.S.R. 'Demokritos' using a wavelength of $\lambda = 1.5437$ Å. X-ray powder diffraction (XRD) data were collected with a D500 SIEMENS diffractometer using CuKα

* Corresponding author. Tel.: +30 210 650 3706; fax: +30 210 653 3431.
E-mail address: KMergia@ipta.demokritos.gr (K. Mergia).

0022-3115/$ - see front matter © 2007 Elsevier B.V. All rights reserved.
doi:10.1016/j.jnucmat.2007.03.267

radiation. Transmission electron microscopy study was carried out using a Philips CM20 TEM equipped with an energy dispersive X-ray spectrometer for chemical microanalysis.

In order to determine the thermal conductivity, the thermal diffusivity, α, and the heat capacity, c_p, were measured. Thermal conductivity values, k, were calculated using the equation

$$k = \alpha c_p d, \tag{1}$$

where d is the bulk density value calculated from the sample's geometry and mass and it was found to be equal to 7.75 g/cm^3.

The thermal diffusivity was measured using the laser flash technique [11]. In the flash method the front face of a small disc-shaped sample is subjected to a short laser burst and the resulting rear face temperature rise is recorded and analysed. The apparatus consists of a laser, a high vacuum system including a bell jar with windows for viewing the sample, a tantalum or stainless steel tube heater surrounding the sample holding assembly, a thermocouple or an infra red detector, appropriate biasing circuits, amplifiers, A/D converters, crystal clocks and a microcomputer based digital data acquisition system capable of accurately taking data in the 40 μs and in longer time domain.

The heat capacity was measured using a standard Perkin–Elmer Differential Scanning Calorimeter with sapphire as the reference material. The standard and the sample were subjected to the same heat flux and the differential power required to heat the sample and the standard at the same rate were determined using a digital data acquisition system. From the mass of the sapphire standard and the sample, the differential power, and the known specific heat of sapphire, the specific heat of the sample is computed.

For the electrical resistivity measurements rectangular samples were cut and subsequently were mechanically thinned and polished in order to remove any damage introduced to the samples by machining. The resistivity was measured by dc four probe method utilizing a computer controlled apparatus and furnace. During the measurement the sample was kept under an inert Ar atmosphere.

The magnetic properties of Eurofer 97 were determined using a Vibrating Sample Magnetometer (VSM) in which the magnetic field of the magnetized sample is used for determining its magnetic moment. The sample, magnetized by an electromagnet, oscillates along the vertical direction with constant frequency, ω, and amplitude, a, and the field, produced by its magnetic moment, m, oscillates with the same frequency. The flux changes, through an appropriate set of pick-up coils, generate a voltage, V, which is proportional to m

$$V = m \times a \times G \times \omega \times \cos(\omega t), \tag{2}$$

where G is a constant depending on the pick-up coils geometry. In order to reduce the noises and achieve a high sensitivity, the output voltage is measured synchronously with the oscillations by means of a lock-in amplifier. The reference signal for the lock-in amplifier is taken from an additional coil, vibrating synchronously with the sample in the magnetic field of an auxiliary permanent magnet. The maximum applied field for the magnetic loops was 1590 kA/m and a Hall sensor was used to monitor the magnetic field values. The magnetization values have been calibrated using the Standard Reference Material SRM 762 Nickel disk. The sample for the magnetic measurements had a mass of 38.03 mg and was in cylindrical form with diameter 1.58 mm and height 2.66 mm.

The magnetic properties, the coercive field, the remanence magnetization and the saturation magnetization, were determined from hysteresis loops measured in the temperature range from room temperature to 900 K. From the magnetic loops the coercive field and the remanence magnetization were obtained, for both branches of the loop, from a least squares fit of the M versus H data in the magnetic field region where a linear behaviour is observed, i.e. between −30 and 30 Oe. The magnetic field values were corrected for the demagnetizing field according to the equation

$$H = H_{\text{ext}} - H_{\text{d}} = H_{\text{ext}} - 4\pi N_{\text{d}}(\chi, \gamma) M d/m, \tag{3}$$

where H_{ext} is the applied external magnetic field in Oe, H_{d} is the demagnetizing field in Oe, N_{d} is the demagnetizing factor which depends on the magnetic susceptibility, χ, and for cylindrical samples on the ratio $\gamma =$ height/diameter, M is the magnetization in emu, d is the density in g/cm^3 and m is the mass of the sample in g. In order to correct for the demagnetizing field, since N_{d} depends on the susceptibility, which is the derivative of the magnetization over the field, one has to iterate Eq. (3) until the corrected field does not change.

3. Results and discussion

3.1. Structure

In Fig. 1 the neutron diffraction data and the corresponding curve obtained by using the Fullprof Rietveld [12] program are presented. The Eurofer 97 as the Fe–Cr

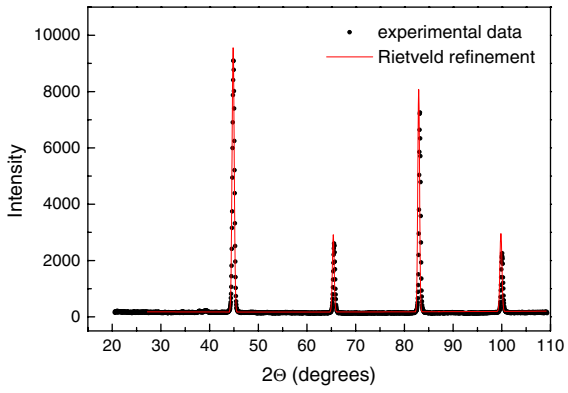

Fig. 1. Neutron diffraction data from Eurofer 97. The continuous line is a fit to the data after Rietveld refinement.

alloys crystallises in the bcc ferromagnetic structure. For the refinement the space group *Im3m* was used and the scattering coefficients of Fe and Cr were weighted with their atomic compositions in Eurofer 97. The atomic cell parameter was found to be 2.842 Å which compares very well with the cell parameter of Fe–9.5 at.%Cr alloy (concentration of Cr very close to that of Eurofer 97) which is 2.862 Å [13].

The TEM measurements showed that the microstructure consists of laths of tempered martensite (Fig. 2(a)). The main precipitation consists of chromium/iron/tungsten $M_{23}C_6$ carbides. The Cr/Fe at.% ratio was measured in the range 1.5–2. The precipitates have a size of 40–200 nm and they are located mainly along grain and lath/subgrain boundaries (Fig. 2(b)).

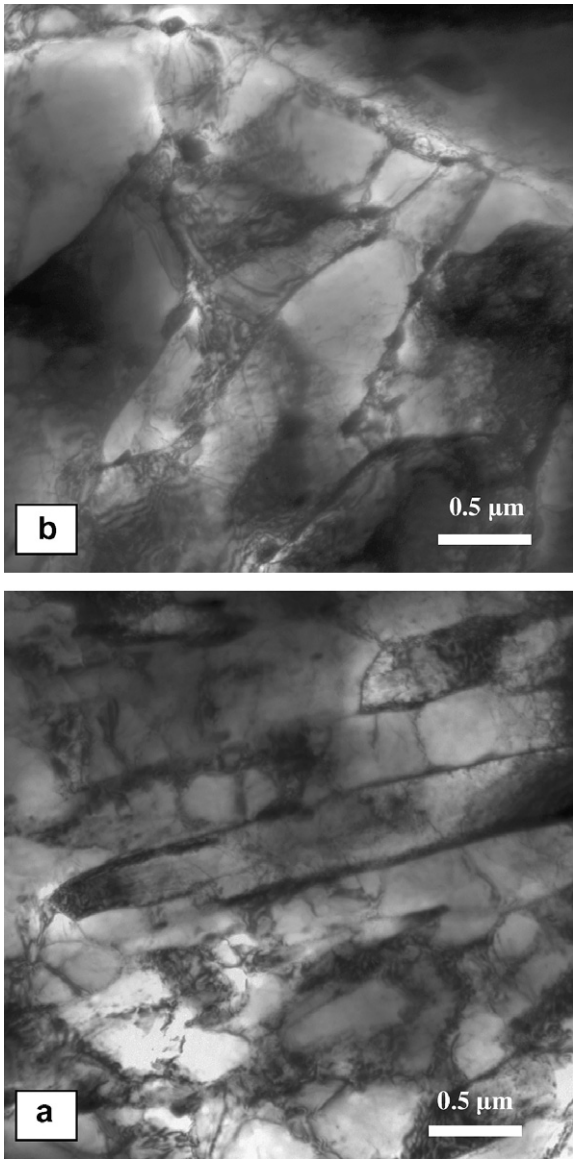

Fig. 2. (a) Bright field overview of the grain/subgrain structure. (b) Typical coarse precipitation at subgrain boundaries of Eurofer 97.

3.2. Thermal, electrical and magnetic properties

3.2.1. Thermal diffusivity, heat capacity and thermal conductivity

The thermal diffusivity, specific heat the thermal conductivity experimental data are presented in Figs. 3–5, respectively. For comparison the same parameters for F82H steel are also presented [14]. The solid lines in these figures are least squares fitted empirical equations to the experimental data. In the formulation of the empirical equations the physical behaviour of the parameters has been taken into account, however, their validity is restricted in the experimental range i.e. 300–900 K for Eurofer 97 and 300–1033 K for F82H.

The thermal diffusivity of Eurofer 97 is much lower than the corresponding values of Fe and Cr, which at room temperature are 0.227 and 0.26 cm^2/s, respectively [15]. The temperature dependence of the thermal diffusivity

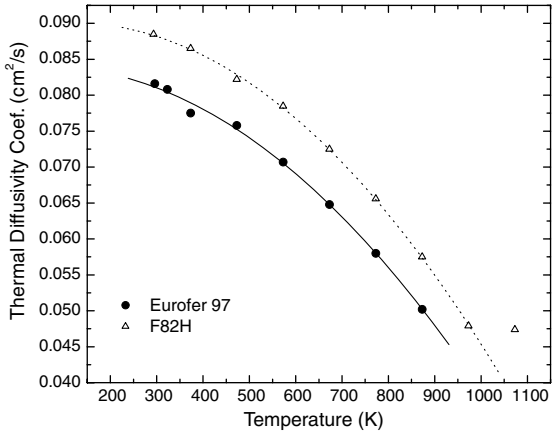

Fig. 3. Thermal diffusivity of Eurofer 97 (solid circles) as a function of temperature. The data for F82H (open triangles) are according to Ref. [14]. The continuous and dotted lines are the least squares fitted equations (4) and (5).

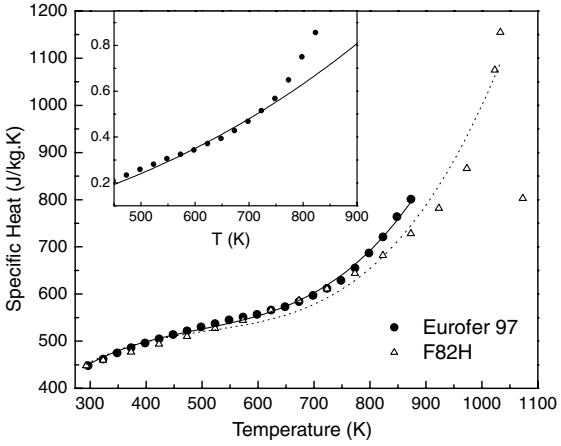

Fig. 4. Specific heat of Eurofer 97 (solid circles) as a function of temperature. The data for F82H (open triangles) are according to Ref. [14]. The continuous and dotted lines are the least squares fitted equations (6) and (7). Insert: Magnetic specific heat for Eurofer 97 (for details see text).

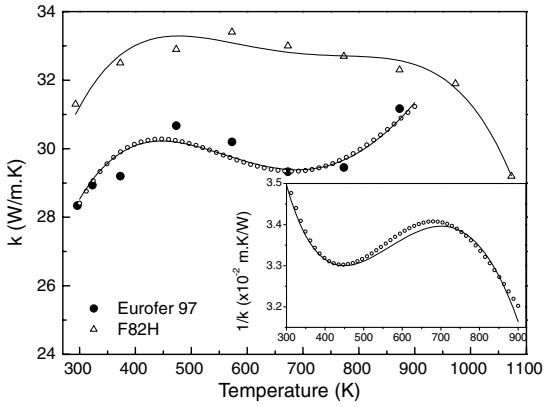

Fig. 5. Thermal conductivity versus temperature. Open circles: Eurofer 97 using Eqs. (1), (4) and (6). Solid circles: Eurofer 97 from the experimental data points of diffusivity and specific heat (Figs. 3 and 4) and using Eq. (1). Open triangles: F82H according to Ref. [14]. The continuous and dotted lines are the least squares fitted equations (10) and (11). Insert: open circles experimental thermal resistivity values of Eurofer 97, continuous line the least squares fitted equation (9).

coefficient for Eurofer 97 and F82H is very similar for temperatures up to 800 K and the mean difference of their values at a given temperature is about 10%. The empirical equations which describe the temperature dependence of the thermal diffusivity of these two alloys is given by the equations:

$$\text{Eurofer 97}: \alpha = 0.08381 + 6.00691 \times 10^{-6} T - 5.09213 \times 10^{-8} T^2, \quad (4)$$

$$\text{F82H}: \alpha = 0.08919 + 1.40507 \times 10^{-5} T - 5.7853 \times 10^{-8} T^2, \quad (5)$$

where α in cm^2/s and T in Kelvin.

The specific heat values for Eurofer 97 and F82H up to 750 K are very close and with a mean difference of about 2%. The difference of specific heats of these two alloys at higher temperatures arises from their different magnetic phase transition temperatures. For the specific heat the empirical equations are as follows:

$$\text{Eurofer 97}: c_p = 2.696T - 0.00496T^2 + 3.335 \times 10^{-6} T^3, \quad (6)$$

$$\text{F82H}: c_p = 2.7319T - 0.00503T^2 + 3.303 \times 10^{-6} T^3 \quad (7)$$

with c_p in J/kg K and T in Kelvin. In the last two empirical equations (6) and (7) the physically expected behaviour at low temperatures i.e. $c_p \to 0$ for $T \to 0$ has been assumed. The specific heat contains three contributions i.e.

$$c_p = c_p^{\text{electronic}} + c_p^{\text{phonon}} + c_p^{\text{magnetic}}. \quad (8)$$

The electronic contribution in the temperature range of this work is very small (the electronic specific heat for Fe becomes comparable to that of phonons at temperatures around 10 K) and thus it can be ignored. The phonon contribution above the Debye temperature (Θ_D for iron is 470 K) can be expressed by the Dulong and Petit law

$$c_p^{\text{phonon}} \approx 3k\frac{N}{V},$$

which for the Eurofer 97 would give the value of 447 J/kg K. Thus the phonon contribution to the specific heat is expected for high temperatures to asymptotically converge to this value. The abrupt increase in the specific heat observed at high temperatures arises from the magnetic contribution as the sample undergoes a second order phase transition from the ferromagnetic to the paramagnetic state. The magnetic contribution to the specific heat can be calculated from the experimental specific heat values by subtracting the Dulong–Petit value (see insert in Fig. 4). Using the mean field theory for the description of the magnetization, the magnetic contribution to the specific heat has been calculated (the magnetic specific heat is proportional to the magnetization and its first derivative and for this calculation $J = 1/2$ and $T_c = 1030$ K have been assumed). This calculation is shown in the insert of Fig. 4 as a solid line together with the experimental data for the magnetic specific heat and a reasonable agreement is observed.

The thermal conductivity for Eurofer 97 has been calculated using Eqs. (1), (4) and (6). The data are presented in Fig. 5 (open circles) together with the individual data points (solid circles) which have been calculated from Eq. (1) and the experimental data points of thermal diffusivity and specific heat as shown in Figs. 3 and 4. In Fig. 5 also the experimental data for F82H are shown. The thermal conductivity of Eurofer 97 at room temperature is around 28 W/m K which is much lower than that of Fe at this temperature which is around 80 W/m K. In the thermal conductivity there are also three contributions as those in the specific heat (see Eq. (8)). In a pure metal the electronic contribution is around thirty times larger than the phononic one. However, in a disordered alloy the phononic and electronic contributions are almost equal. The thermal resistivity ($W = 1/k$) has a term varying as T^2 due to electron scattering by lattice vibrations, a term varying as $1/T^x$ describing the scattering of the electrons by the impurities and a term which depends on the magnetic electron scattering. All these contributions are expressed with the equation

$$W = \frac{1}{k} = 1.27 \times 10^{-8} T^2 + \frac{1.267}{T^{0.66}} + 0.074\left(\frac{T}{T_c}\right)^2\left(1 - \frac{T}{T_c}\right), \quad (9)$$

where W in (m K)/W, T in K and $T_c = 1030$ K. The constants in Eq. (9) have been found by a least squares fit to the experimental data (see insert in Fig. 5). For practical applications the thermal conductivity least squares fitted empirical equations for Eurofer 97 and F82H steel are:

$$\text{Eurofer 97}: k = T(0.190706 - 4.3053 \times 10^{-4} T + 3.817 \times 10^{-7} T^2 - 1.158 \times 10^{-10} T^3), \quad (10)$$

$$\text{F82H}: k = T(0.2130 - 4.9606 \times 10^{-4} T + 4.980 \times 10^{-7} T^2 - 1.837 \times 10^{-10} T^3), \quad (11)$$

where k in W/m K and T in Kelvin.

3.2.2. Specific electrical resistivity

The results of the specific electrical resistivity measurements as a function of temperature are presented in Fig. 6. It is observed that the electrical resistivity, ρ, increases with temperature in a parabolic manner. A least squares fit to the data gives the following empirical equation:

$$\rho = 8.536 + 0.1484T - 2.84 \times 10^{-5}T^2, \quad (12)$$

where ρ is the specific electrical resistivity in $10^{-8}\Omega$ m = μΩ cm and T is the temperature in K. This kind of parabolic temperature dependence has been found in other steel alloys such as AISI 305 [16]. The specific resistivity can be written, assuming the applicability of Mathiessen's rule as

$$\rho(T) = \rho_0 + \rho^{\text{phonon}}(T) + \rho^{\text{magnetic}}(T),$$

where ρ_0 is the impurity scattering of the conduction electrons. The phonon scattering in the temperature range studied is expected to vary proportionally to temperature. The magnetic scattering of conduction electrons can be expressed as [17]

$$\rho^{\text{magnetic}}(T) = G\left(1 - \frac{\langle \mathbf{S} \rangle^2}{S(S+1)}\right), \quad (13)$$

where the factor G depends on the spin of the magnetic atom [18] and the variation of $\langle \mathbf{S} \rangle$ with temperature may be derived from the magnetization versus temperature curve. Using Eq. (18) for the magnetization and the value of G from Ref. [17] corresponding to experimentally determined mean magnetic moment of $1.85\mu_B$/atom (see section 3.2.3) the resistivity arising from the magnetic scattering of the conduction electrons has been calculated and it is presented in the insert of Fig. 6. If from the total specific resistivity the magnetic contribution is subtracted we find that the resistivity arising from the impurities and phonon scattering is given as

$$\rho_0 + \rho^{\text{phonon}}(T) = 12.256 + 0.137T. \quad (14)$$

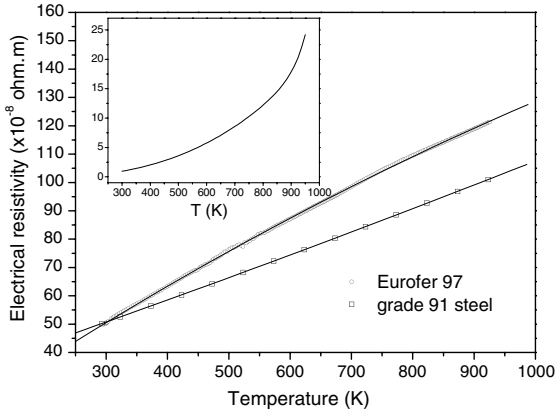

Fig. 6. The specific electrical resistivity of Eurofer 97 versus temperature. The continuous line is the least squares fitted equation (12). The open squares correspond to the electrical resistivity values from grade 91 steel [15]. Insert: the resistivity corresponding to the magnetic scattering of conduction electrons (see text for details).

3.2.3. Magnetic properties

The transition temperature, T_c, from the ferromagnetic to paramagnetic state has been determined by the measurement of the magnetization versus temperature and in a field of 12 Oe. From the linear extrapolation of the magnetization near the transition region the value of the transition temperature was determined as 1030 K.

Measurements of hysteresis loops were carried out from room temperature to 900 K and to a maximum field of 1000 kA/m. The hysteresis loops were corrected for demagnetization effects according to Eq. (3). The corrected hysteresis loop at room temperature is presented in Fig. 7.

The methodology for the determination of the coercive field, H_c, and of the remanence, M_r has been discussed in section 2. In order to obtain the saturation magnetization, M_s, we assume that the magnetization near saturation is expressed as

$$M = M_s + \frac{A}{H^2}. \quad (15)$$

From a plot of the magnetization versus $1/H^2$ the saturation magnetization is determined from the intercept of the least squares fitted line. The temperature dependence of the coercive field, the remanence and the saturation magnetization, are presented in Figs. 8–10. For comparison the corresponding data for the steel F82H [14] are also presented. We observe that the coercive field for F82H for all the temperatures reported is 1.5 times larger than that for Eurofer 97. An average 5% difference is observed in M_s between Eurofer 97 and F82H, which is almost constant over the temperature range reported for both alloys. The values of M_r for F82H are not shown in Fig. 9 because in Ref. [14] it is not stated whether the correction for the demagnetizing field has been applied. It has to be noted that the demagnetizing field correction has a significant effect on the remanence magnetization values but not on the coercive field values.

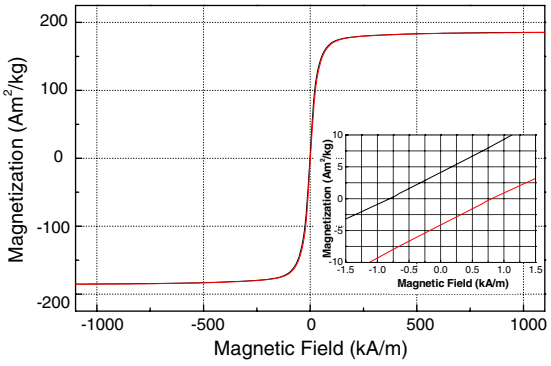

Fig. 7. Hysteresis loop of Eurofer 97 at room temperature. Insert: the centre of the hysteresis loop.

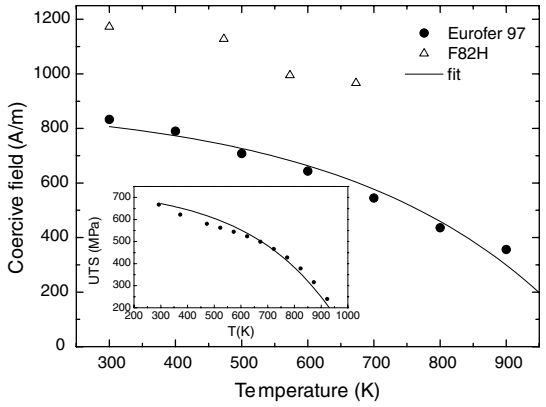

Fig. 8. The temperature dependence of the coercive field for Eurofer 97 (solid circles). The open triangles correspond to F82H data according to Ref. [14]. The continuous line is the least squares fitted equation (16). Insert: Solid circles UTS data for Eurofer 97 according to reference [9], continuous line equation (19).

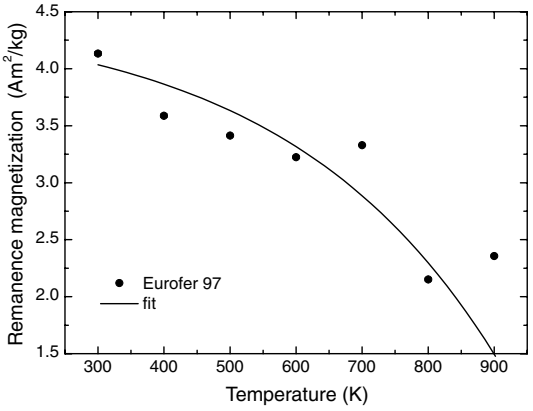

Fig. 9. The temperature dependence of the remanence magnetization for Eurofer 97 (solid circles). The continuous line is the least squares fitted equation (17).

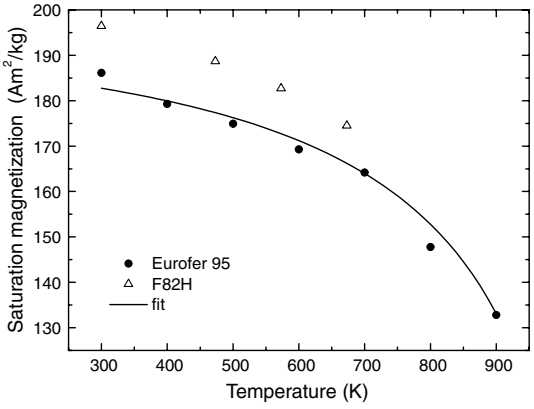

Fig. 10. The temperature dependence of the saturation magnetization for Eurofer 97 (solid circles). The open triangles correspond to F82H data according to Ref. [14]. The continuous line is the least squares fitted equation (18).

The empirical equations describing the coercive field, the remanence and the saturation magnetization for Eurofer 97 are as follows:

$$H_c = 900\{1 - \exp[-3.2(1 - T/T_c)]\}, \quad (16)$$

$$M_r = 4.5\{1 - \exp[-3.2(1 - T/T_c)]\}, \quad (17)$$

$$M_s = 196\{1 - \exp[-3.2(1 - T/T_c)^{0.5}]\}, \quad (18)$$

where H_c in (A/m), M_r in (A m^2/kg), M_s in (A m^2/kg), T in Kelvin and $T_c = 1030$ K. In the above expressions the physically expected behaviour that these parameters should vanish as T approaches T_c has been incorporated. The fitted curves using the above equations are presented as solid lines in Figs. 8–10, The saturation magnetization at $T = 0$ corresponds to a magnetic moment of $1.85\mu_B$/atom. This value agrees very well with experimental and calculated values [19] of a Fe–Cr alloy with the same Cr content as Eurofer 97. The maximum permeability values measured for Eurofer 97 were in the range 39–53 for the temperatures 293 and 900 K, respectively.

3.2.4. Discussion on the difference of the physical properties between Eurofer 97 and F82H steels

At a first glance the alloys F82H and Eurofer 97 appear very similar and one might expect them to have closer values of their physical properties than those experimentally determined. Differences in the atomic concentrations of the additives, mainly Cr, in the solution and tempering temperature and in the cooling rates result into atomically different magnetic structures and precipitation microstructure. The structural dissimilarities are manifested in different values in the physical properties of these two alloys and mainly in their temperature dependence. In the following paragraphs an account will be given on how the physical properties of these two alloys and generally Fe-rich Cr alloys are correlated with their structural parameters. This discussion will be based on the preceding sections in which the underlying physics for each physical property were given.

The atomic magnetic structure of Fe–Cr alloys plays an important role in describing the miscibility gap, the anomalous stability of Fe-rich Cr alloys and the phase transformations [20]. The mixing enthalpy for the ferromagnetic bcc Fe–Cr, calculated by the density functional theory method EMTO-CPA, is negative for Cr concentrations below 10at.%Cr which explains the anomalous stability of these alloys for compositions around 6–9 at.%Cr [21]. The negative value of mixing enthalpy for Cr concentrations below 10 at.%Cr is of magnetic origin due to the long range ferromagnetic order (the mixing enthalpy in the paramagnetic state does not exhibit this behaviour). The magnetic properties of these alloys are strongly dependent on the Cr atomic concentration and Eurofer 97 and F82H have of about 1.2 at.%Cr content difference (9.5 at.%Cr in Eurofer 97 and 8.3 at.%Cr in F82H). The 1.2 at.%Cr increase in the Eurofer 97 has as consequence the increase of the lattice constant and a reduction of the net magnetic

moment [21]. The reduction of the magnetic moment explains the lower by 5% values of saturation magnetization of Eurofer 97 when compared with F82H (see Fig. 10). The net magnetic moment reduction results in a lower transition temperature from the ferromagnetic to paramagnetic phase in Eurofer 97 than that of F82H [20]. The T_c for F82H has not been measured however it is apparent from the specific heat measurements presented in Fig. 4 that it is higher than that of Eurofer 97.

The specific heat values (Fig. 4) of these two alloys up to 750 K are very close (within 2%) which implies that the phononic contribution to the specific heat is almost the same for both alloys (no large differences are to be expected since both alloys have the same crystal structure and very close lattice constants). The divergence of the specific heats at higher temperatures arises from the magnetic contribution to the specific heat and the different T_c of the alloys. As it has been pointed out in section 3.2.1, if there was no ferromagnetic to paramagnetic phase transition, the specific heat of both alloys at high temperatures would be around the value given by the Dulong–Petit law. Also the magnetic transition explains the difference in the temperature dependence of the electrical resistivity. We observe from Fig. 6 that the electrical resistivity values of the two alloys at room temperature, which is far away from their magnetic phase transitions, are very close. As the temperature increases the resistivity is determined by the combined effects of atomic scattering and spin-disorder scattering. The spin dependent electron scattering accounts for a large percentage of the resistivity increase with temperature (see insert in Fig. 6) and thus the temperature dependent resistivity difference between these two alloys.

Lastly we have to explain the difference in thermal conductivity and coercive field between F82H and Eurofer 97. These two properties depend on both the degree of the magnetic order but also on the nano and microstructure of these two steels. The presence of a higher concentration of the grain refining Ta in Eurofer 97 results in a finer prior austenite grain size in Eurofer 97 in comparison with F82H. Also differences between these two alloys in the degree of the precipitation and the chemical composition of the precipitates have been observed [22]. The differences in the microstructure are also reflected in a different mechanical behaviour of the two steels. In this context it should be emphasized the peculiar bulk modulus behaviour at low Cr concentrations [23].

At low temperatures, where the magnetic phase transition temperature plays minor role, the thermal conductivity of F82H is around 10% higher than that of Eurofer 97 and this difference cannot be attributed to the different magnetic order of these two steels. If we analyze the thermal conductivity data of F82H according to Eq. (9) we find that Eurofer 97 has a lower impurity scattering but a higher phononic scattering. The change of the strength of the scattering mechanisms could be attributed predominantly to that Eurofer 97 has a finer grain structure which has as a result the reduction of the electron and phonon free mean path [24].

Coercivity and remanence are structure sensitive magnetic properties. Coercivity arises from the irreversible movement of the domain walls. Domain wall structure, spatial variation of internal stress (5% increase in strain in steels results to 30% increase in the coercive field [25]), inclusions, dislocations play an important role in the coercive field value. Even small volume fractions of precipitates and either interstitial or substitutional solutes dramatically increase the coercive field [26]. The available experimental data on the magnetic properties on Eurofer 97 and F82H makes it impossible to correlate the difference of the coercive field between these two alloys to a specific microstructure difference. In order to evaluate the influence of the microstructure on the coercive field values hysteresis loops of heat treated samples, under which the microstructure change, are needed. However, is known that Vicker's hardness and Ultimate Tensile Strength (UTS) are correlated with coercive field [27,28]. It is interesting to correlate the temperature dependence of UTS and that of the coercive field. The experimental data of UTS versus temperature [9] can be described by the equation

$$\mathrm{UTS} = 750\{1 - \exp[-3.2(1 - T/T_c)]\}, \tag{19}$$

where UTS is in MPa (see insert in Fig. 8). This equation has the same functional form as Eq. (16) which describes the temperature dependence of the coercive field. This correspondence shows that the coercive field and UTS are well correlated. This important correlation between mechanical properties and magnetic properties needs to be further investigated since it is known that neutron irradiation changes both the magnetic [29] and mechanical properties of this steel.

4. Summary and conclusions

The Eurofer crystallizes in the bcc ferromagnetic structure with the main microstructure consisting of laths of tempered martensite. The thermal, electrical and magnetic properties of Eurofer 97 steel were determined in the temperature range from room temperature up to 900 K. The experimental data are described by empirical equations and are compared with the corresponding values for the F82H steel. The specific heat data for Eurofer 97 and F82H are very close for temperatures up to about 800 K, whereas the diffusivity data differ of about 10%. As a result a difference of about 9% is observed in the thermal conductivities. The specific electrical resistivity of Eurofer 97 is compared with that of grade 91 steel. The electrical resistivities are very close at room temperature but diverge at high temperatures due to the different magnetic phase transition temperatures. The coercive field and the saturation magnetization of Eurofer 97 are systematically lower than those of F82H for the whole temperature range of the measurements. The versus temperature values of the coercive field and UTS for Eurofer 97 are well correlated.

Notwithstanding that the structural differences between the Eurofer 97 and F82H are not profound, the temperature dependence of the physical properties of these two alloys is dissimilar. The temperature dependent differentiation arises mainly from the different magnetic transition temperature and to some degree from the different solutes and precipitate microstructure. The study of the physical properties after thermal treatments and neutron irradiations will provide valuable information on the correlation of physical properties and structure and consequently in understanding on how structure affects the mechanical and irradiation resistance behaviour of this important for Fusion applications steel.

Acknowledgements

The work was carried out under support of EFDA contract TTMS-002-D5. We thank Dr R. Lindau for the provision of the specimens and Dr F. Tavassoli and Dr S. Messoloras for helpful discussions and comments.

References

[1] A. Kohyama, A. Hishinuma, D.S. Gelles, R.L. Klueh, W. Dietz, K. Ehrlich, J. Nucl. Mater. 233–237 (1996) 138.
[2] M. Gasparoto, R. Andreani, L.V. Boccaccini, A. Cardella, G. Federici, L. Giancarli, G. LeMarois, D. Maisonnier, S. Malang, A. Moeslang, Y. Poitevin, B. van der Schaaf, M. Victoria, Fusion Eng. Des. 66–68 (2003) 129.
[3] B. van der Schaaf, F. Tavassoli, C. Fazio, E. Rigal, E. Diegele, R. Lindau, G. LeMarois, Fusion Eng. Des. 69 (2003) 197.
[4] R. Andreani, E. Diegele, W. Gulden, R. Lässer, D. Maisonnier, D. Murdoch, Y. Poitevin, The EFDA Team, Fusion Eng. Des. 81 (2006) 25.
[5] E. Lucon, P. Benoit, P. Jacquet, E. Diegele, R. Lässer, A. Alamo, R. Coppola, F. Gillemot, P. Jung, A. Lind, S. Messoloras, P. Novosad, R. Lindau, D. Preininger, M. Klimiankou, C. Petersen, M. Rieth, E. Materna-Morris, H.-C. Schneider, J.-W. Rensman, B. van der Schaaf, B.K. Singh, P. Spaetig, Fusion Eng. Des. 81 (2006) 917.
[6] A. Paùl, E. Alves, L.C. Alves, C. Marques, R. Lindau, J.A. Odriozola, Fusion Eng. Des. 75–79 (2005) 1061.
[7] H. Bolt, V. Barabash, W. Krauss, J. Linke, R. Neu, S. Suzuki, N. Yoshida, ASDEX Upgrade Team, J. Nucl. Mater. 329–333 (2004) 66.
[8] A.-A.F. Tavassoli, A. Alamo, L. Bedel, L. Forest, J.-M. Gentzbittel, J.-W. Rensman, E. Diegele, R. Lindau, M. Schirra, R. Schmidt, H.C. Schneider, C. Petersen, A.-M. Lancha, P. Fernandez, G. Filacchioni, M.F. Maday, K. Mergia, N. Boukos, Baluc, P. Spätig, E. Alves, E. Lucon, J. Nucl. Mater. 329–333 (2004) 257.
[9] R. Lindau, A. Möslang, M. Schirra, Fusion Eng. Des. 61&62 (2002) 659.
[10] S. Jitsukawa, M. Tamura, B. van der Schaaf, R.L. Klueh, et al., J. Nucl. Mater. 307–311 (2002) 179.
[11] J. Parker, R.J. Jenkins, C.P. Butler, G.L. Abbot, J. Appl. Phys. 32 (1961) 1679.
[12] J. Rodriguez-Carvajal, Physica B 192 (1993) 55.
[13] W.B. Pearson, A Handbook of Lattice Spacings and Structure of Metals and Alloys, Pergamon Press, Belfast, 1958, p. 532.
[14] F. Tavassoli, DEMO Interim structural design criteria. Ref. N,T.-DMN/DIR 2002.
[15] H. Stamm, U. Holzwarth, F. Lakestani, R. Valiev, V. Prozenzano, A. Volkan, J. Nucl. Mater. 283–287 (2000) 597.
[16] X. Tan, P.P. Conway, F. Sarvar, J. Mater. Process. Tech. 168 (2005) 152.
[17] P.G. de Gennes, J. Friedel, J. Phys. Chem. Solids 4 (1958) 71.
[18] R.J. Weiss, A.S. Marotta, J. Phys. Chem. Solids 9 (1959) 302.
[19] P. Olssom, I.A. Abrikosov, L. Vitos, J. Wallenius, J. Nucl. Mater. 321 (2003) 84.
[20] G.J. Ackland, Phys Rev. Lett 97 (2006) 015502.
[21] P. Olsson, I.A. Abrikosov, J. Wallenius, Phys. Rev. B 73 (2006) 104416.
[22] P. Fernández, A.M. Lancha, J. Lapeña, M. Hernández-Mayoral, Fusion Eng. Des. 58&59 (2001) 787.
[23] P. Olsson, I.A. Abrikov, L. Vitos, J. Wallenius, J. Nucl. Mater. 321 (2003) 84.
[24] M. Omini, A. Sparavigna, Phys. Rev. B 61 (2000) 6677.
[25] S.M. Thomson, B.K. Tanner, J. Magn. Magn. Mater. 83 (1990) 221.
[26] L.J. Dykstra, in: A.E. Berkowitz, E. Kneller (Eds.), Magnetism and Metallurgy, Academic Press, 1969.
[27] Jai Won Byeon, S.I. Kwun, Mater. Lett. 58 (2003) 94–98.
[28] S.S.M. Tavares, M.R. da Silva, J.M. Neto, J. Alloy Compd. 313 (2000) 168–173.
[29] D.G. Park, E.J. Moon, D.J. Kim, S.H. Chi, J.H. Hong, Physica B 327 (2003) 315.